Microscopic magnetic traps for neutral atoms

J. D. Weinstein* and K. G. Libbrecht†
12-33 California Institute of Technology, Pasadena, California 91125
(Received 13 April 1995)

We describe planar and mostly planar current geometries for constructing microscopic magnetic traps for neutral atoms. These geometries are well-suited for fabrication from superconductors using standard microfabrication techniques. Magnetic-field gradients greater than 5×10^5 G/cm, and field curvatures greater than 10^8 G/cm^2 can be produced in microscopic traps. Trap loading could be accomplished by constructing a nested series of traps, and compressing atom clouds from larger traps into smaller ones. In the smallest magnetic microtraps the motional ground-state energy of atoms in the trap can exceed the recoil energy from resonant photons, which may allow direct laser cooling to the trap ground state. If a number of atoms can be simultaneously cooled to the ground state, the resulting "Bose clusters" should exhibit interesting optical behavior, since their spatial extent would be less than the resonant light wavelength.

PACS number(s): 33.80.Ps

I. INTRODUCTION

Purely magnetic traps for confining neutral atoms, molecules, and elementary particles have the appealing feature that the trapped particles suffer no wall collisions, and are thus extremely well isolated from their external environment. To date, magnetic traps have been demonstrated for neutrons [1], atomic hydrogen [2], and a variety of laser-cooled alkali-metal atoms [3]. These traps were all of macroscopic size, typically in the range of 1–100 cm, and were constructed from room-temperature coils, superconducting coils or permanent magnets. A particularly intriguing application of such traps is in attempts to observe Bose-Einstein condensation (BEC) in gases of spin-polarized atoms. Considerable effort is currently underway to achieve this goal, either using atomic hydrogen precooled in a dilution refrigerator, or using alkali-metal atoms precooled using laser-cooling techniques. In both cases a promising route is to load precooled atoms into a magnetic trap, and then further cool the sample using forced evaporative cooling to achieve phase-space densities high enough for BEC [4].

A BEC gas is expected to exhibit an unusual optical behavior, which is readily probed using resonant laser radiation [5]. The optical response depends strongly, however, on the extent of the trap ground state Δx_{ground} in comparison to the wavelength of the resonant light λ_{res}. Since all magnetic traps that have been constructed to date have used macroscopic magnetic coils and permanent magnets, they produce fairly modest field gradients and curvatures, giving traps with $\Delta x_{\text{ground}} \gg \lambda_{\text{res}}$. Elementary scaling considerations suggest that much higher field gradients and curvatures can be realized using microscopic superconducting traps, enough to achieve traps with $\Delta x_{\text{ground}} < \lambda_{\text{res}}$. By virtue of the uncertainty principle, the energy-level splitting of a trap with $\Delta x_{\text{ground}} < \lambda_{\text{res}}$ is greater than the recoil energy from a single resonant photon $E_{\text{recoil}} = \hbar^2 k^2 / 2M$, where $k = 2\pi/\lambda_{\text{res}}$ and M is the particle mass. Thus direct laser cooling to the ground state may be possible in such a trap.

A number of different magnetic-field configurations are suitable for trapping neutral particles, including magnetostatic traps [6], which can trap weak-field-seeking states only, and dynamical traps [7,8], which can trap either weak- or strong-field seekers. Magnetostatic "multipole" traps, such as quadrupole and hexapole traps, are the simplest to construct, have the largest trap depths for a given current density, and are well matched for loading from a quadrupole magneto-optical trap. However, atoms trapped in multipole traps have a spatially varying polarization vector and can suffer Majorana transitions to untrapped states upon passing near the field zero at the trap center.

The Ioffe configuration [6] includes a bias field, so the polarization vector of trapped atoms is nearly spatially invariant near the trap center, and Majorana transitions are not possible. However, the Ioffe trapping potential is relatively shallow, and only very cold atoms can be trapped.

Dynamical magnetic traps [7,8] are extremely shallow, but are an attractive option for magnetically trapping strong-field-seeking states. Dynamical traps are thus capable of trapping the lowest-energy atomic state, which in a finite field is always strong-field seeking [9]. This is desirable since the cross section for spin-flip collisions between ground-state atoms in a bias field can be energetically forbidden at low temperatures.

Magnetic fields generated from current-carrying wires typically scale as I/S, where I is the wire current and S is the characteristic size of the system. Similarly, magnetic-field gradients and curvatures scale as I/S^2 and I/S^3 respectively. This scaling, along with the practical limits to attainable wire-currents (see the Appendix), indicate that smaller magnetic traps can be made more tightly confining than large ones. This leads us to consider the construction of microscopic magnetic traps in order to produce extremely large magnetic-field gradients and curvatures. Since it is difficult to fabricate free-standing three-dimensional microstructures, we consider here the fabrication of traps using micron-scale superconducting circuits confined to a planar substrate.

*Electronic address: jonathan@cco.caltech.edu
†Electronic address: kgl@sundog.caltech.edu

II. MULTIPLE MAGNETOSTATIC TRAPS

A macroscopic quadrupole trap is most easily made using two coaxial coils of equal sizes, with equal currents flowing in opposite directions. The two-dimensional analog of this arrangement is two coplanar, coaxial coils, with unequal currents flowing in opposite directions. This forms a quadrupole trap with its center (with $|\mathbf{B}|=0$) on axis above the substrate. A more practical arrangement is a single current ring and a bias field, where the latter is generated external to the substrate. This single-coil+bias arrangement is capable of steeper and deeper traps than the planar two-coil geometry. Figure 1 shows a comparison of these three types of quadrupole traps.

We first find the quadrupole trap configuration that provides the deepest magnetic trap, assuming a minimum coil radius $R_{\min}$ and maximum current $I_{\max}$. We assume the wire width is much smaller than $R_{\min}$, which will be approximately valid for Type I superconductors, where there is little advantage in making the wire width much greater than its thickness (see the Appendix). Because the wires for such a trap will most likely be deposited onto a surface, we impose the additional constraint that the trap center not intersect the plane of the wires. For a ring current I and radius R, the single-ring quadrupole trap depth is optimized for a bias field $B_{\text{bias}}=\mu_0 I/4R$, giving a maximum trap depth of

$$E_{\max}=\mu B_0=k_B T_{\max}=\frac{\mu\mu_0 I_{\max}}{4R_{\min}},$$

where μ is the particle magnetic moment. Note that the trap depth is greater for greater $I_{\max}$ and smaller $R_{\min}$. Note also that because the trap depth scales only as $I_{\max}/R_{\min}$, microscopic quadrupole traps will not be substantially deeper than their macroscopic counterparts (see the Appendix).

Optimizing the trap instead for magnetic-field gradient at the trap center yields an optimal configuration for a bias field of

$$B_{\text{bias}}=\frac{\mu_0}{2}\left(\frac{4}{5}\right)^{3/2}\frac{I}{R}\simeq 0.36\frac{\mu_0 I}{R},$$

which gives a maximum axial field gradient at the trap center of

$$B'_{\max}=\frac{\partial|\mathbf{B}|}{\partial z}=\frac{3}{4}\left(\frac{4}{5}\right)^{5/2}\frac{\mu_0 I_{\max}}{R^2_{\min}}\simeq 0.43\frac{\mu_0 I_{\max}}{R^2_{\min}}.$$

For $\mu=\mu_B$, a Bohr magneton, $I_{\max}=1$ A, and $R_{\min}=10$ μm, this gives a maximum trap depth of $T_{\max}=21$ mK, and $B'_{\max}=5.4\times 10^5$ G/cm.

Like the quadrupole trap, the hexapole trap [6] also has $|\mathbf{B}|=0$ at the trap center, but the hexapole trap's field varies quadratically (although not isotropically) about the center. Near the center of a hexapole trap we have

$$B_z=C(z^2-\tfrac{1}{2}\rho^2),$$

$$B_\rho=-Cz\rho,$$

$$B_\phi=0,$$

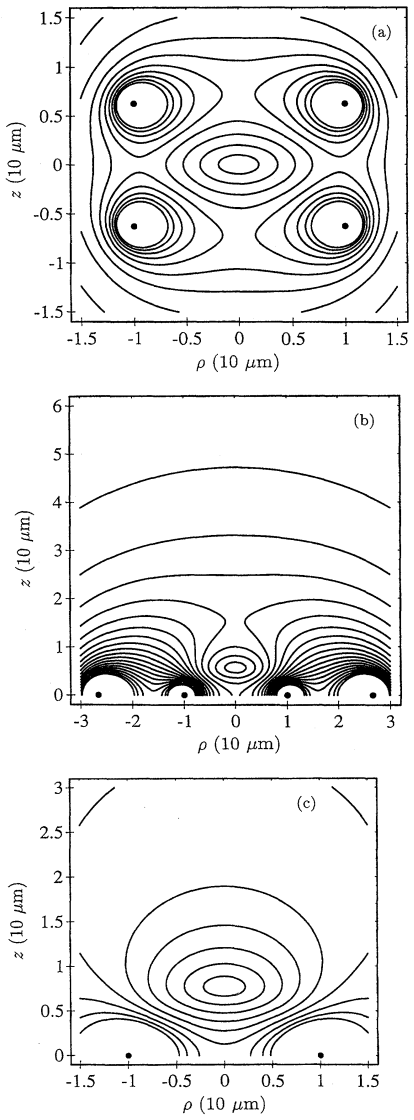

FIG. 1. Contours of $|\mathbf{B}|$ for (a) the three-dimensional, two-coil quadrupole trap, (b) the planar two-coil trap, and (c) the planar one-coil and bias field trap. All have been optimized for maximum trap depth. For each trap the maximum current is $I_{\max}=1$ A, and the radius of the smallest coil is $R_{\min}=10$ μm. For (a), contours are every 100 G (beginning at 100 G) and the loops lie in the planes $z=\pm 0.627R$. For (b), contours are every 25 G, $I_1=-0.533I_2$, and $R_2=2.66R_1$. For (c), contours are every 50 G and $B_{\text{bias}}=-314$ G.

where C is a constant specific to a given trap configuration.

With planar currents the hexapole trap can be fabricated from three coplanar current loops, or from two loops and a bias field. The latter configuration again yields deeper and more tightly confining traps for a given $I_{\max}$ and $R_{\min}$. For the two-coil configuration, the trap depth is optimized for

$$I_1=-0.422I_2,$$

$$R_2=2.37R_1,$$

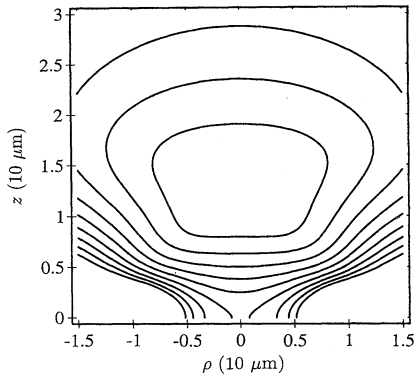

FIG. 2. Contours of $|\mathbf{B}|$ for a planar hexapole trap, optimized for maximum trap depth. Contours are drawn at 20 G intervals, with $R_{\min}=10$ μm and $I_{\max}=1$ A. $I_1=-0.422I_2$, $R_2=2.37R_1$, and $B_{\text{bias}}=119$ G.

$$B_{\text{bias}}=0.0946\frac{\mu_0 I_2}{R_1},$$

giving $C=0.0601\mu_0 I_2/R_1^3$ and a depth of $B_0=0.0946\mu_0 I_2/R_1$. Magnetic-field contours for this trap are shown in Fig. 2. Optimizing for field curvature, we find

$$I_1=-0.512I_2,$$

$$R_2=1.48R_1,$$

$$B_{\text{bias}}=0.109\frac{\mu_0 I_2}{R_1},$$

which gives $C=0.102\mu_0 I_2/R_1^3$. For $I_{\max}=1$ A, $R_{\min}=10$ μm, we have $T_{\max}=8.0$ mK and $B''_{\max}=2.6\times10^8$ G/cm^2. For $\mu=\mu_B$ and a mass of 1 amu, the trap with maximum field curvature has an equivalent harmonic-oscillator energy-level splitting of $\Delta E/k_B=9.1$ μK along the axis, and $\Delta E/k_B=6.5$ μK in the radial direction. These scale as $\Delta E \propto \sqrt{\mu I_{\max}/MR_{\min}^3}$ where M is the particle mass.

III. IOFFE TRAPS

The Ioffe trap is a magnetostatic trap with a nonzero value of $|\mathbf{B}|$ near the trap center, and $|\mathbf{B}|$ increasing quadratically away from the center. Thus trapped atoms have a nearly spatially invariant spin vector, and losses from Majorana transitions are prevented. Nonplanar current geometries for Ioffe traps include two current loops surrounded by four "Ioffe bars," the so-called "baseball" trap, and the "Yin-Yang" trap [6].

Some possible planar geometries for Ioffe traps include: (a) three concentric half loops; (b) two half loops with an external bias field; (c) one half loop, one full loop, and a bias field; (d) two full loops with a bias field, and external Ioffe bars, which are shown in Fig. 3. The first of these, which we will refer to as Ioffe (a) is essentially a planar analog of the nonplanar Ioffe trap with two loops and four Ioffe bars. The Ioffe (b) configuration replaces one of the loops with a bias field, as was done above for the multipole traps. The Ioffe (c) configuration is similar to the Ioffe (b) but provides a steeper trapping potential on axis and weaker trapping in the perpendicular directions; this makes an overall deeper trap with a greater energy-level splitting for a given $I_{\max}$ and $R_{\min}$. The Ioffe (d) is a hybrid configuration, which uses external (macroscopic) Ioffe bars to produce the 2-dimensional quadrupole field, while deriving the on-axis trapping fields from two loops and a bias field. This is a reasonable trapping configuration because macroscopic coils, particularly from Type II superconductors, can generate quadrupole fields that are nearly as large as those from microscopic coils (see the Appendix).

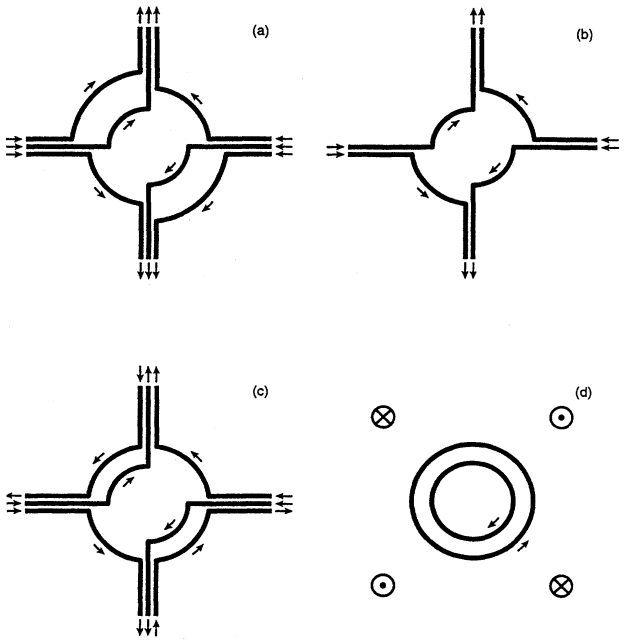

FIG. 3. Four planar (and pseudoplanar) Ioffe trap configurations, as described in the text.

Near the center of the Ioffe trap the magnetic field can be written, to the order of r^2, as

$$B_z=C_1(z^2-\tfrac{1}{2}\rho^2)+B_{\text{offset}},$$

$$B_\rho=-C_1 z\rho+C_2\rho\cos(2\phi),$$

$$B_\phi=-C_2\rho\sin(2\phi),$$

where C_1 and C_2 are constants specific to a given trap configuration. Thus

$$B\approx B_{\text{offset}}+C_1z^2+(C_2^2/B_{\text{offset}}-C_1)\rho^2/2,$$

which gives a stable trap if $0<B_{\text{offset}}<C_2^2/C_1$.

Figure 4 shows contours of constants $|\mathbf{B}|$ for the Ioffe (c) configuration, optimized for maximum field curvature. For a given $I_{\max}$ and $R_{\min}$, the axial energy-level splitting for this configuration is maximized for

$$R_2=1.50R_1,$$

$$I_2=I_1,$$

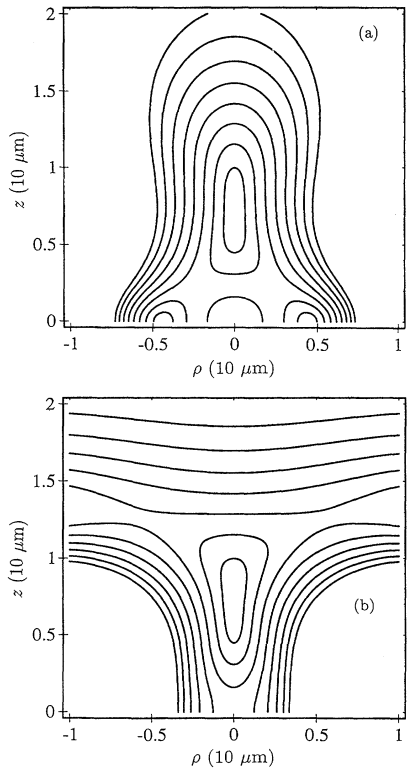

FIG. 4. Contours of $|\mathbf{B}|$ for the Ioffe (c) trap configuration, optimized for maximum axial field curvature. The two views show (a) in a plane with $\phi=45°$ (passing through two Ioffe-c wires), and (b) the $\phi=-45°$ plane. The wires lie in the plane $z=0$ and are centered around $\rho=0$. As before, $R_{\min}=10$ μm and $I_{\max}=1$ A, and contours are drawn at 10-G intervals. For this configuration $I_1=I_2$, $R_2=1.50R_1$, and $B_{\text{bias}}=140.4$ G, giving $B_{\text{offset}}=1$ G.

giving $C_1=1.28\times10^8$ G/cm^2, $C_2=1.54\times10^5$ G/cm, and $B_{\text{offset}}=B_{\text{bias}}-0.111\mu_0 I_1/R_1$. For $I_{\max}=1$ A, $R_{\min}=10$ μm, the on-axis energy-level splitting for 1 amu is $\Delta E/k_B=9.1$ μK, which again scales as $\Delta E \propto\sqrt{\mu I_{\max}/MR_{\min}^3}$. For ^{133}Cs, $\Delta E/k_B=0.79$ μK, which is 7.9 times as large as the recoil limit temperature, while for ^{7}Li, $\Delta E/k_B=3.4$ μK, which is 1.1 times the recoil limit.

The energy-level splitting in the radial direction is dependent on B_{offset}. For the same $I_{\max}$ and $R_{\min}$ as above, the splitting in the radial directions for 1 amu is 88 μK for $B_{\text{offset}}=1$ G, which decreases with increasing B_{offset}.

The currents in the Ioffe (d) trap have the same optimum values as was found for the hexapole trap above. The trapping potential in the axial and radial directions can be varied by independently adjusting the ring currents and the strength of the external quadrupole field. Figure 5 shows an isotropic Ioffe (d) trap optimized for maximum field curvature.

IV. DYNAMICAL TRAPS

Because a static magnetic field cannot have a local maximum in free space, magnetostatic traps can only trap atoms in weak-field-seeking states. Since these states are not minimum-energy states in the field, spin-flip collisions can

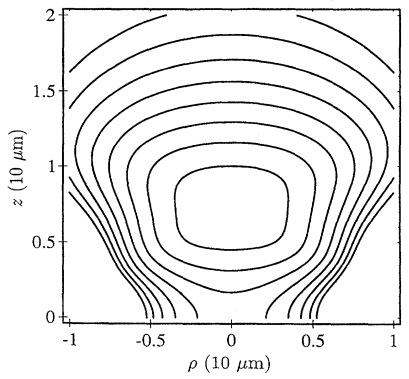

FIG. 5. Contours of $|\mathbf{B}|$ for the Ioffe (d) configuration optimized for maximum axial field curvature, with external Ioffe bars characteristics such that the trap is isotropic around its center. $R_{\min}=10$ μm and $I_{\max}=1$ A, and contours are drawn at 10 G intervals. For this configuration $I_1=0.512I_2$, $R_2=1.481R_1$, and $B_{\text{bias}}=-138$ G, giving $B_{\text{offset}}=1$ G. The Ioffe bars give $\partial B_\rho/\partial\rho=1.96\times10^4$ G/cm at the trap center.

produce strong-field-seeking states that are ejected from the trap. Dynamical traps, in contrast, can be used to trap atoms in either weak- or strong-field-seeking states [7,8].

The simplest planar dynamical trap with a nonzero bias field consists of two coaxial rings with sinusoidal currents that vary as $I(t)=I_0\cos(\omega t)$, producing a magnetic field $\mathbf{b}(\mathbf{x},t)=\mathbf{b}(\mathbf{x})\cos(\omega t)$, plus a static axial bias field B_0. In the limit that $B_0\gg|\mathbf{b}|$, we can expand the total magnetic field to give $|\mathbf{B}|\approx B_0+b_z(\mathbf{x},t)$ to lowest order in $|\mathbf{b}|/B_0$. This results in a force on the trapped particle,

$$\mathbf{F}(\mathbf{x},t)=\mu\frac{\partial}{\partial\mathbf{x}}b_z(\mathbf{x})\cos(\omega t).$$

For $\omega^2\gg\mu_0\mu_B I/4\pi mR^3$, the effective potential for the time-averaged motion of the particle is [10]

$$U=\frac{F^2}{4m\omega^2}.$$

Including the constraint on ω, the trap depth then scales as $(I_{\max}/R_{\min})$ and the energy-level splitting as $\Delta E \propto\sqrt{\mu I_{\max}/MR_{\min}^3}$.

Optimizing the trap for depth, for a given maximum current and minimum radius, we find the maximum depth occurs for

$$I_1=-0.432I_2,\quad R_2=1.63R_1.$$

If we take

$$\omega^2=100\frac{\mu_0\mu I}{4\pi mR^3},$$

then for $I_{\max}=1$ A, $R_{\min}=10$ μm, and $\mu=\mu_B$, we have $\omega=650$ kHz for ^{133}Cs and a trap depth of 10 μK. While this is quite shallow, owing to the unfavorable $(I_{\max}/R_{\min})$ scal-

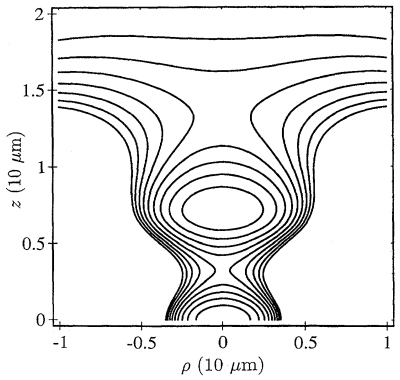

FIG. 6. Contours of the effective potential in the dynamical trap described in the text, optimized for energy-level splitting. $R_{\min}=10$ μm, $I_{\max}=1$ A, $R_2=1.48R_1$, $I_1=-0.512I_2$, and $\omega=650$ kHz. Contours are drawn at 2-μK intervals.

ing, laser cooling can produce samples this cold, and three-dimensional traps with comparable depths have been successfully used [8].

Optimizing for level splitting gives

$$I_1=-0.512I_2, \quad R_2=1.48R_1,$$

which produces a splitting for 1 amu of $\Delta E=0.52$ μ K in the radial direction and $\Delta E=1.0$ μK on axis. The trapping field produced by this optimization (see Fig. 6) is only slightly different from that of the trap optimized for depth.

V. DISCUSSION

From the above we see that extremely high field gradients and curvatures can be generated using superconducting microstructures, which can then be used for neutral atom trapping. With high trap resonance frequencies and the low loss rates associated with cryogenic atom traps [11], single-atom oscillators with mechanical quality factors of $Q\geq 10^7$ should be attainable. With sufficiently high magnetic-field curvatures, trapping neutral atoms in the Lamb-Dicke regime may be possible, as has been achieved in optical lattices [12]. In contrast to optical lattices, however, loading microscopic traps to high densities might be done efficiently by constructing a nested series of magnetic traps on a single substrate, and progressively compressing the atoms into the smallest traps. The Ioffe (d) trap is especially well-suited for such a procedure. With additional evaporative cooling during the compression, one might achieve sufficient phase-space density to observe quantum statistical effects in an atomic sample confined to size smaller than the resonant optical wavelength. With sufficiently strong trapping, so that the trap energy-level splitting is greater than the recoil limit, direct laser cooling to the trap's ground state may also be possible.

Microfabrication of planar traps from niobium foil can be done commercially down to sizes of a few microns, and submicron photolithography of niobium is frequently used in construction on Josephson junctions for superconducting quantum interference devices (SQUIDs) and sub-mm radiation detection. In addition to the simple traps considered here, other trap geometries can be constructed, such as miniature storage rings [9]. More complex two-dimensional arrays of superconducting wires might also be used effectively as atom-optical elements. SQUID detection of the magnetic field generated by a trapped spin-polarized atomic sample might also be realized in microscopic traps [13].

ACKNOWLEDGMENTS

This work was supported by gifts from M. Jacobs and the Hale Foundation. J.D.W. acknowledges support from the California Institute of Technology.

APPENDIX

An important consideration in building microscopic magnetic traps is the maximum current that can be supported by wires of various materials, and how the maximum current scales with size. We consider here three classes of materials: normal metal wires, Type I superconductors, and Type II superconductors.

For a normal metal wire, the maximum current is limited by the necessity of removing the ohmic heating produced by the current. If we consider a wire of radius r carrying a current I, and remove the ohmic heating via conduction in the wire, then we have approximately

$$\frac{I}{r}\lesssim\left(\frac{2\pi^2\kappa\Delta T_{\max}}{\rho}\right)^{1/2},$$

where κ is the thermal conductivity, ρ is the electrical resistivity, and $\Delta T_{\max}$ is the maximum allowable temperature difference between the wire and its surroundings. For room-temperature copper, taking $\Delta T_{\max}=50$ °C, $\kappa=500$ W m^{-1} K^{-1}, and $\rho=2\times10^{-8}$ Ω m, we have $(I/r)\lesssim 5\times10^6$ A/m. The actual value achieved with macroscopic wires may be much smaller than this value, owing to practical considerations associated with carrying the heat away (e.g., with cooling water).

Cooling pure copper to 4 K reduces its electrical resistivity by 2–4 orders of magnitude (depending on the purity of the material), while κ experiences only a moderate increase. Thus low-temperature microscopic copper wires on a conducting substrate might be used to achieve higher values of I/r. In this case an additional constraint appears, namely the cooling capacity of the refrigeration system. For a 1-W capacity we have typically $I^2/r\gtrsim 10^9$ A^2/m.

The current through a wire made from a Type I superconductor is limited by the requirement that the magnetic field generated at the wire's surface not exceed the critical field, giving

$$\frac{I}{r}\gtrsim\frac{2\pi B_{\text{crit}}}{\mu_0}$$

for a cylindrical wire. For Nb, with $B_{\text{crit}}=0.20$ T, we have $I/r\gtrsim 1.0\times10^6$ A/m. While this value is less than the maximum I/r for refrigerated copper, the absence of ohmic heating in the superconductor is a significant practical advantage.

Forming the wire into a wide strip does not result in a substantial improvement for Type I superconductors, as was shown by Huebener, Kampwirth, and Clem [14]. Using a wire with an elliptical cross section (which can be solved analytically), they found

$$\frac{I_{\max}}{L_x+L_y}<\left[\frac{B_{\mathrm{crit}}L_y}{L_x+L_y}-B_{\mathrm{app}}\right]\Big/(4\times10^{-7}\ \mathrm{T\ m/A}),$$

where L_x and L_y are the major and minor axes of the ellipse, and B_{app} is an applied field. Using this approximation for a strip of Type I superconductor with $L_x>L_y$, as might be deposited on a substrate, we see that for $B_{\mathrm{app}}=0$ the maximum current that can be carried is roughly proportional to the thickness of the deposited layer, and independent of its width.

Type II superconductors operated at fields above the lower critical field are limited by a maximum current density $\rho_{\max}$ thus giving

$$\frac{I}{r^2}<\pi\rho_{\max}$$

for a cylindrical wire. Taking $\rho_{\max}=4\times10^9$ A/m^2, a typical value for NbTi, we have $I/r^2\gtrsim1.2\times10^{10}$ A/m^{-2}.

From these calculations we see Type II superconductors can achieve higher values of I/r than Type I or copper wires if $r\gtrsim100$ μm; thus Type II superconductors are preferred for macroscopic coils. For microstructures, however, Type I superconductors or copper wires are superior. Wires made from Nb deposited on a planar substrate should carry 1 A if the deposited thickness is approximately 2 μm or greater [14].

[1] K. J. Kugler, W. Paul, and U. Trinks, Phys. Lett. B **72**, 422 (1978).

[2] T. W. Hijmans, O. J. Luiten, I. D. Setija, and J. T. M. Walraven, J. Opt. Soc. Am. B **6**, 2235 (1989); J. M. Doyle, J. C. Sandberg, N. Masuhara, I. A. Yu, D. Kleppner, and T. J. Greytak, *ibid.* **6**, 2244 (1989).

[3] A. Migdall, J. Prodan, W. Phillips, T. Bergeman, and H. Metcalf, Phys. Rev. Lett. **54**, 2596 (1985); V. S. Bagnato, G. P. Lafyatis, A. G. Martin, E. L. Raab, R. N. Ahmad-Bitar, and D. E. Pritchard, *ibid.* **58**, 2194 (1987); C. R. Monroe, E. A. Cornell, C. A. Sackett, C. J. Myatt, and C. E. Wieman, *ibid.* **70**, 414 (1993); J. J. Tollet, C. C. Bradley, C. A. Sackett, and R. G. Hulet, Phys. Rev. A **51**, R22 (1995).

[4] H. F. Hess, G. P. Kochanski, J. M. Doyle, N. Masuhara, D. Kleppner, and T. J. Greytak, Phys. Rev. Lett. **59**, 672 (1987); O. J. Luiten, H. G. C. Werij, I. D. Setija, M. W. Reynolds, T. W. Hijmans, and J. T. M. Walraven, *ibid.* **70**, 544 (1993); W. Petrich, M. H. Anderson, J. R. Ensher, and E. A. Cornell, in *Atomic Physics 14: Proceedings of the Fourteenth International Conference on Atomic Physics, Boulder, 1994*, edited by D. J. Wineland, C. E. Wieman, and S. J. Smith (AIP, New York, 1995); K. B. Davis, M. O. Mewes, M. A. Joffe, and W. Ketterle, *ibid.*

[5] H. D. Politzer, Phys. Rev. A **43**, 6444 (1991); B. Svistunov and G. Shlyapnikov, Zh. Eksp. Theor. Fiz. **97**, 821 (1990) [Sov. Phys. JETP **70**, 460 (1990)]; **98**, 129 (1990) [**71**, 71 (1990)]; J. Javanainen, Phys. Rev. Lett. **72**, 2375 (1994); L. You, M. Lewenstein, and J. Cooper, Phys. Rev. A **50**, R3565 (1994).

[6] T. Bergeman, G. Erez, and H. Metcalf, Phys. Rev. A **35**, 1535 (1987).

[7] R. V. E. Lovelace, C. Mehanian, T. J. Tommila, and D. M. Lee, Nature **318**, 30 (1985).

[8] E. A. Cornell, C. Monroe, and C. E. Wieman, Phys. Rev. Lett. **67**, 2439 (1991).

[9] W. Ketterle and D. E. Pritchard, Appl. Phys. B **54**, 403 (1992).

[10] L. D. Landau and E. M. Lifshitz, *Mechanics* (Pergamon, Oxford, 1960), pp. 93–94.

[11] P. A. Willems and K. G. Libbrecht, Phys. Rev. A **51**, 1403 (1995); K. Helmerson, A. Martin, and D. E. Pritchard, J. Opt. Soc. Am. B **9**, 483 (1992).

[12] P. Verkerk, B. Lounis, C. Salomon, C. Cohen-Tannoudji, J.-Y. Courtois, and G. Grynberg, Phys. Rev. Lett. **68**, 3861 (1992).

[13] J. T. M. Walraven and I. F. Silvera, Physica **107B**, 517 (1981); M. B. Ketchen *et al.*, IEEE Trans. Magn. **25**, 1212 (1989).

[14] R. P. Huebener, R. T. Kampwirth, and J. R. Clem, J. Low Temp. Phys. **6**, 275 (1972).